Influence of Coulomb correlations on gain and stimulated emission in (Zn,Cd)Se/Zn(S,Se)/(Zn,Mg)(S,Se) quantum-well lasers

P. Michler, M. Vehse, J. Gutowski, M. Behringer, and D. Hommel
Institut für Festkörperphysik, Universität Bremen, P.O. Box 330440, D-28334 Bremen, Germany

M. F. Pereira, Jr. and K. Henneberger
Theoretische Physik III, Universität Rostock, P.O. Box 999, D-18051 Rostock, Germany
(Received 18 December 1997; revised manuscript received 12 February 1998)

The influence of Coulomb correlations on gain and stimulated emission in (Zn,Cd)Se/Zn(S,Se)/(Zn,Mg)(S,Se) quantum-well lasers is studied under stationary conditions. Systematic temperature-dependent measurements under application of different spectroscopic techniques were performed. Optical gain is measured by means of the variable stripe-length method, whereas excitonic bleaching under lasing conditions is analyzed through two-beam photoluminescence excitation (PLE) spectroscopy. Furthermore, complementary low-density single-beam PLE spectra are recorded in order to study the temperature dependence of the heavy-hole exciton peaks. The experimental data as a whole are shown to be inconsistent with any of the usually quoted excitonic models for lasing in II-VI heterostructures. The experiments are more adequately explained by a strongly correlated electron-hole plasma described by Bethe-Salpeter-like equations for the optical response and recombination rates in the excited medium. The nonequilibrium Green's-function approach used consistently includes, at a microscopic level, band structure, quantum-confinement, and many-body effects. [S0163-1829(98)02528-4]

I. INTRODUCTION

The understanding of the physical mechanisms giving rise to laser emission in wide-gap II-VI semiconductors has attracted much interest in the past.[1–14] Whereas electron-hole plasma recombination is accepted as the gain mechanism in conventional III-V semiconductors, the larger exciton binding energy in wide-gap II-VI semiconductors gives rise to a considerable influence of Coulomb correlation on gain and stimulated emission. From the theoretical point of view, there are several attempts discussed in order to account for the lasing mechanism in II-VI semiconductors. Exciton-related lasing, based on inelastic scattering processes in a dense exciton gas such as exciton-LO-phonon, exciton-exciton, and exciton-electron interaction, was initially proposed. This was discussed by Bénoit à la Guillaume *et al.*,[1] and a detailed theoretical description in the polariton picture has been given by Haug and Koch.[2]

A second process relies on the inhomogeneous broadening of the exciton resonance in localizing systems such as ZnCdSe/ZnSe quantum wells and was discussed by Ding *et al.*[3,4] Here, the inhomogeneous broadening of the exciton resonance provides an effective multilevel system and exciton population relaxation effects are the cause for gain.

The third possible mechanism discussed by Klingshirn and Haug[5] is the biexciton decay into one photonlike and a second excitonlike polariton. Indeed, biexcitons are favored in recent publications to explain optical gain at low temperatures in undoped, ultrapure (Zn,Cd)Se/ZnSe multiple quantum wells (MQW's) (Ref. 6) and ZnSe/Zn(S,Se)/(Zn,Mg)(S,Se) (Ref. 7) separate confinement heterostructures.

Electron-hole plasma recombination is assumed[8] to be the dominant mechanism for lasing even at low temperatures in shallow $Zn_{0.9}Cd_{0.1}Se/ZnSe$ quantum-well structures. At higher temperatures beyond 80 K this mechanism is also favored for ZnSe/Zn(S,Se) superlattices.[9]

The influence of Coulomb correlation on gain-current characteristics[4,11] and optical probe spectra[12] at 300 K has recently been discussed. However, a consistent model that describes properly the experimentally observed absorption and/or gain, luminescence, and two-beam photoluminescence excitation spectroscopy for arbitrary temperatures was still not available.

In this paper, we present experimental results on excitonic optical nonlinearities and gain in (Zn,Cd)Se/Zn(S,Se)/(Zn,Mg)(S,Se) quantum-well lasers applying two different spectroscopic techniques. In order to obtain insight into the lasing process, we have studied the excitonic bleaching under lasing conditions using a pump-and-probe photoluminescence excitation spectroscopy (PLE) of the stimulated emission.[15] Additionally, systematic temperature-dependent gain measurements have been performed. The redshifts of the gain maxima and the excitonic resonances as a function of temperature are compared. We show that a model of a strongly correlated electron-hole plasma, which is presented in detail in Ref. 17, can give a consistent interpretation of the experimental data, especially at higher temperatures. The paper is organized as follows. Section II gives details about the samples and experiments. The theory used is summarized in Sec. III. Experimental results are presented in Sec. IV and are compared and contrasted to numerical solutions of the equations in Sec. V.

II. SAMPLES AND EXPERIMENTAL DETAILS

The investigated undoped separate-confinement heterostructures lasers were grown by molecular-beam epitaxy

(MBE). The II-VI layers were grown on GaAs substrates and buffers in a twin chamber MBE system EPI 930 for separate III-V and II-VI growth. The GaAs buffer layer thickness was about 300 nm. The samples were grown on full 2 in. wafers and no chemical etching was performed, prior to growth. The start was performed on a mixed $c(4\times4)/(2\times4)$ As stabilized GaAs surface at a temperature of about 320 °C. The growth of the II-VI layers was initialized using a migration enhanced epitaxy kind regime during which Zn was kept open all the time and Se was opened for 2 sec, than closed for 4 sec. After 20 of these cycles, the growth was continued with normal MBE growth. The defect density was in the low 10^5 cm^{-2} and the layers were fully strained. The $ZnS_{0.06}Se_{0.94}$ waveguide layers with an overall thickness of 170 nm are embedded in $Zn_{0.85}Mg_{0.15}S_{0.27}Se_{0.73}$ cladding layers being 1 μm thick. One structure contains five 5-nm-thick $Zn_{0.8}Cd_{0.2}Se$ wells while the other structure possesses six 3-nm-thick $Zn_{0.8}Cd_{0.2}Se$ wells separated by 10-nm-thick $ZnS_{0.06}Se_{0.94}$ barriers, respectively. The samples were optically excited by 10-ns pulses of an excimer pumped dye laser at a repetition rate of 50 Hz. Thus, the created carriers can be considered to be in a steady state. The excitation energy was chosen to be resonant with the energy of the first light-hole exciton in the wells. For the gain measurements the variable stripe-length method (VSLM) (Ref. 16) was used. The stripe width was 10 μm and the stripe length was controlled by a stepper motor and varied between 20 and 200 μm. The amplified spontaneous emission (ASE) emitted from the sample edge was dispersed by a double monochromator and detected by an optical multichannel analyzer. No polarizer was used. The modal gain $g_{\mathrm{mod}}(E)$ at energy E is extracted from

$$\frac{I_1(E,L_1)}{I_2(E,L_2)}=\frac{\exp(g_{\mathrm{mod}}(E)L_1)-1}{\exp(g_{\mathrm{mod}}(E)L_2)-1} \tag{1}$$

with $L_{1,2}$ two different stripe lengths, $I_{1,2}$ the respectively measured intensities of the ASE, or from direct fits to

$$I(L,E)=\frac{I_{\mathrm{sp}}(E)}{g_{\mathrm{mod}}(E)}[\exp(g_{\mathrm{mod}}(E)L)-1] \tag{2}$$

with $I_{\mathrm{sp}}(E)$ the spontaneous emission intensity. Special care was taken to avoid gain saturation effects in the gain spectra. By plotting the ASE intensity as a function of the stripe length, gain saturation is indicated by a deviation of the ASE intensity from that given by Eq. (2) at long stripe lengths. Gain saturation is found to set in for $g_{\mathrm{mod}}L>3$ on the high-energy side of the gain spectra in these samples. The gain spectra presented below are therefore measured for stripe lengths shorter than those for which saturation effects occur.

In order to get information about the lasing process, we have studied the excitonic bleaching under lasing conditions using pump-and-probe photoluminescence excitation spectroscopy (PLE) of the stimulated emission.[15] This spectroscopic technique reveals only those absorption channels that contribute to the stimulated emission being detected as luminescence from the sample edge. For this technique, two synchronously pumped dye lasers are used. Both laser beams were focused on top of the sample as stripes to support stimulated emission along the stripe direction. One (pump) is fixed in energy and creates a certain carrier density within the active layer of the sample. The second dye laser (probe) is tuned to scan the PLE spectrum. The probe laser lies temporally and spatially within the pump pulse to explore the lasing-relevant sample absorption. It has been thoroughly checked that the stimulated emission wavelength stays independent of the excitation energy of the pump laser across the tuned wavelength spectrum. The probe excitation intensity was kept constant throughout the PLE scan by means of a calibrated continuous-adjustable attenuator. It is chosen large enough to keep the sample in the stimulated-emission regime during the whole scan over the energy range of the investigated absorption, which is essential for a reliable measurement. In this case, the PLE spectrum is a qualitative measure of the relative efficiency of the laser excitation channels and, thus, not identical but somewhat related to the absorption behavior under lasing conditions. In conjunction with a microscopic theory that considers the quantitative change of the absorption coefficient under the actual pump conditions, detailed information about the optical nonlinearities under lasing conditions can be obtained.

Furthermore, low-density single-beam PLE spectra are measured to study the temperature dependence of the heavy-hole exciton peaks. Complementary continuous-wave absorption measurements at 2 K show that the absorption spectra have nearly the same spectral shape as the PLE spectra. In particular, no shift of peaks is observed if PLE and absorption spectra are compared.

III. THEORY

The Green's-function approach used here, the details of which are given in Ref. 17, consistently describes light emission and absorption, treating the relevant quasiparticles, describing the excited semiconductor medium (carriers, photons, and plasmons) within the same fully-quantum-mechanical footing.[18,19] The quantum confinement and valence-band coupling, which are used as input for the many-body calculations, require the diagonalization of the corresponding Luttinger Hamiltonian.[20] We consider only constituent materials in which the band gap is sufficiently large to decouple the conduction bands, which are then parabolic. The dispersion relations for a typical quantum well are illustrated in Fig. 1, together with the effective TE components of the dipole moment, which give rise to optical selection rules. The influence of Coulomb correlations beyond the random phase approximation (RPA) is contained in the transverse polarization function. The retarded component P^r includes spectral information while the carrier recombination rates are described by the backward propagator, $P^<$. The detailed analysis given in Ref. 17 shows how these two quantities are related. The Wannier exciton is obtained in the limiting case of vanishing carrier populations in the Bethe-Salpeter equation for the polarization function. This corresponds to the experimental findings presented in Sec. V. However, with a finite carrier density, the Coulomb potential is screened, the band gap is modified, and carrier-carrier scattering takes place. The Bethe-Salpeter equation no longer corresponds to a simple excitonic picture and now describes a many-particle system that in this sense goes beyond the exciton picture. Taking the results obtained for $P^<$ in Ref. 17, we can derive the emitted light field intensity $I(\omega)$. If we

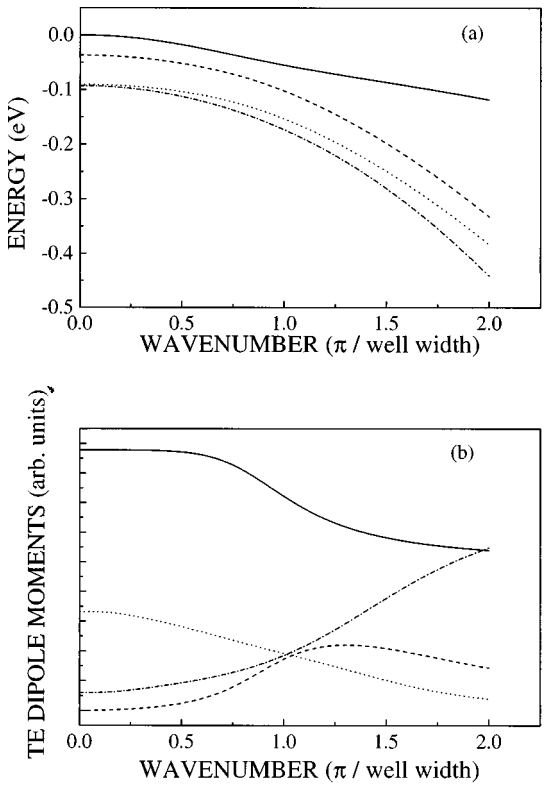

FIG. 1. (a) Nonparabolic dispersion relations for a 5 nm $Zn_{0.8}Cd_{0.2}Se/ZnSe$ QW. From top to bottom the bands correspond at $k=0$ to HH1, HH2, LH1, and HH3. (b) Corresponding TE dipole moments.

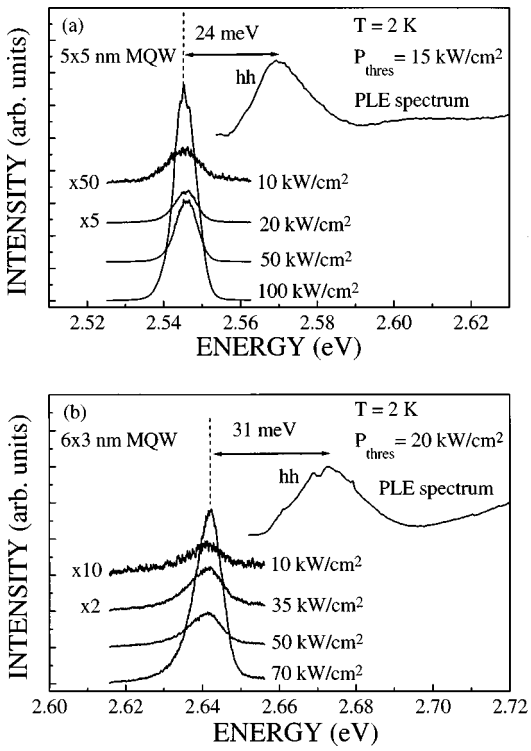

FIG. 2. Evolution of the laser edge emission from below threshold to well above threshold at 2 K for the (a) 5×5 nm and the (b) 6×3 nm sample. The low-density PLE spectra are also shown for reference.

assume the samples to be antireflection coated, so that resonator effects play no role, $I(\omega)$ per unit length can be simplified,[19,21]

$$I(\omega)\sim\hbar\omega^2/4\pi^2 c i P^{<}(\omega), \tag{3}$$

while the absorption reads

$$\alpha(\omega)\sim c/[2\omega\sqrt{\epsilon(\infty)}]\mathrm{Im}\ P^{r}(\omega). \tag{4}$$

IV. EXPERIMENTAL RESULTS

The evolution of the edge emission spectra from pump intensity values below threshold to those well above threshold and the low-density PLE spectra of the two laser samples at 2 K are displayed in Fig. 2. The threshold is defined as the pump intensity where an abrupt increase of the output intensity occurs with increasing pump intensity. Pumping into the energy of the light-hole exciton, the threshold densities are 15 kW/cm^2 and 20 kW/cm^2 for the laser structures with 5×5 nm and 6×3 nm active layers, respectively. The rather similar threshold pump intensities for both samples correspond to an estimated carrier density of about 10^{11} cm^{-2} (assuming a typical carrier lifetime of 100 ps and an absorption coefficient of 3×10^4 cm^{-1} for both samples). This value is well below the Mott density[22] [$n_s\approx(1-3)\times10^{12}$ cm^{-2}] for the present QW structures. The emission spectra from the sample edge do not show any significant shift of the emission maxima if excitation density is varied from below to well above threshold density. However, a considerable redshift between the stimulated emission and the low-density PLE maxima is observed, being larger for the 3-nm wells (31 meV) than for the 5-nm wells (24 meV) at 2 K [see Figs. 2(a) and 2(b)].

The resonance linewidths in the PLE spectra amounting to 13.2 meV (18.5 meV) for the 5-nm (3-nm) heavy-hole (hh) resonances at 2.569 eV (2.673 eV) can be attributed to alloy composition and well thickness fluctuations. The binding energies E_b of the quasi-2D excitons in the 5×5 nm and the 6×3 nm QW systems are approximately 32 and 36 meV,[23] respectively. Temperature-dependent PLE spectra show well-defined excitonic features between 2 and 300 K (see Fig. 3). This points to the fact that the exciton binding energies are larger than the LO-phonon energy of 30 meV (Ref. 4) in these QW systems, so that direct dissociation of excitons into continuum states is energetically not possible by LO-phonon-exciton scattering. For comparison, we have plotted calculated PLE spectra in Fig. 3, which will be discussed in detail in Sec. V.

Figure 4(a) shows the two-beam PLE spectra of the 6×3 nm sample. The excitation energy of the pump laser coincides with the light-hole exciton transition, and stimulated emission is detected at 2.642 eV. The spectrum recorded for pump off exhibits a strong heavy-hole exciton peak at about 2.673 eV. With increasing pump intensity, one observes a bleaching and a broadening of the excitonic absorption. Figure 4(b) shows the two-beam spectra for the same sample at 75 K, where the excitation energy of the pump laser is 2.715 eV and the stimulated emission is detected at 2.638 eV. The spectrum for pump off exhibits a strong exciton peak at 2.666 eV. One observes a similar

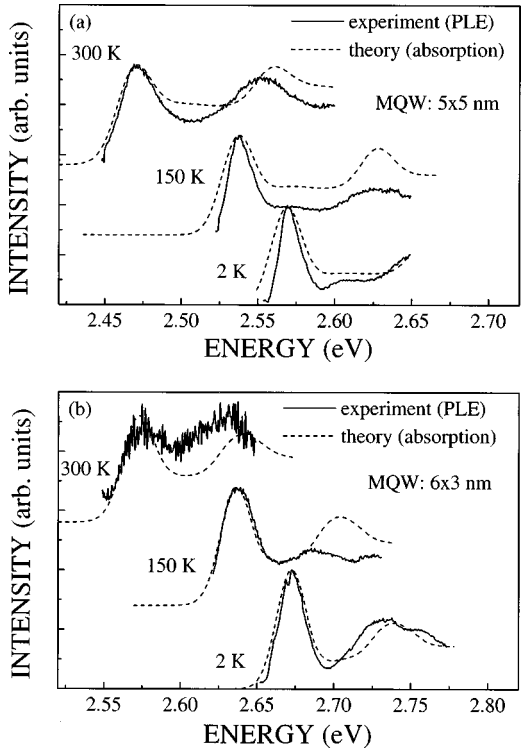

FIG. 3. Measured PLE spectra (solid) and calculated linear absorption spectra (dashed) at three different temperatures for the (a) 5×5 nm and the (b) 6×3 nm sample.

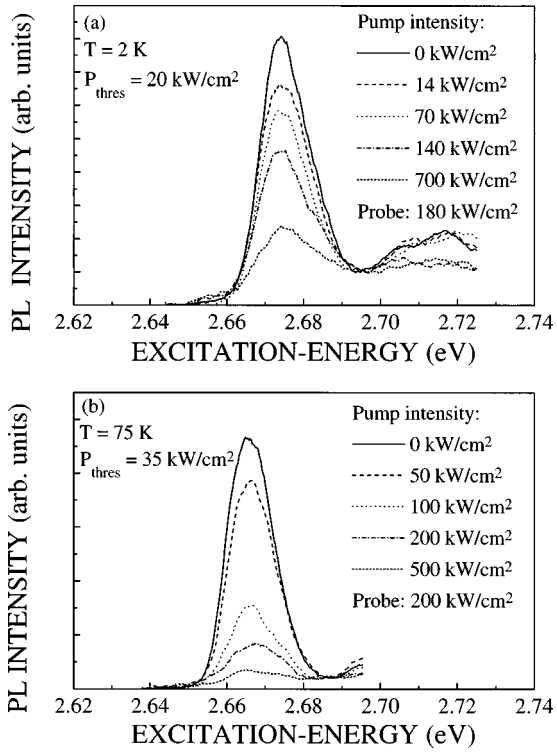

FIG. 4. (a) Two-beam PLE spectra of the 6×3 nm sample at 2 K under different pump intensities from zero to well above threshold density. The luminescence background caused by the pump laser is subtracted in each spectrum. The spectra are normalized to the probe PLE intensity at 2.695 eV. (b) Respective two-beam PLE spectra at 75 K.

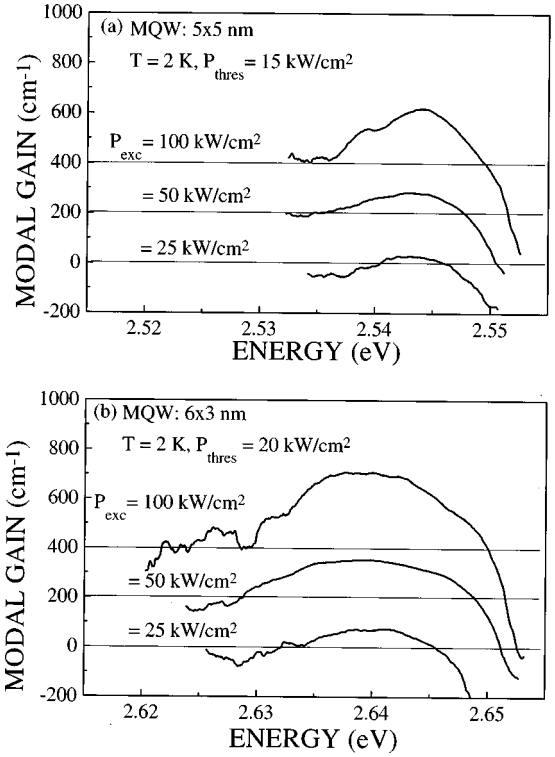

FIG. 5. Measured optical gain spectra at various pump power levels for the (a) 5×5 nm and the (b) 6×3 nm sample.

bleaching and broadening behavior of the excitonic resonance with increasing pump intensity as for the 2 K measurement. Clearly, the excitonic enhancement is more stable at lower temperature. However, it is remarkable that a pronounced excitonlike peak is remaining visible for pump intensities well above the threshold densities for both temperatures. This result points to the influence of Coulomb correlations being still strong at densities sufficient to yield stimulated emission.

In Fig. 5, gain spectra (obtained by the stripe-length method, see Sec. II) are shown for the 5×5 nm and 6×3 nm sample at three different excitation densities. The excitation energy is resonant to the energy of the light-hole exciton for both samples (identical to the energy of the pump laser in the two-beam experiment). The following features are observed for increasing excitation intensity. The transition of modal gain into absorption shifts to higher energies. The peak energy of the modal gain remains nearly constant compared to the width of the gain spectra. The low-energy tail of the gain spectra shifts to lower energies. The gain curves of the 6×3 nm sample are broader than those of the 5×5 nm sample at comparable excitation densities. This feature corresponds to the findings in the linear PLE spectra shown in Fig. 2. It is due to the more pronounced inhomogeneous broadening in the thinner QW's.

Furthermore, one notices that the modal gain is clearly larger for the 6×3 nm sample than for the 5×5 nm sample at corresponding excitation intensities. To compare the material gain $g(E)$ of the two samples, its relation to the measured modal gain $g_{\mathrm{mod}}(E)$ has been used,

$$g_{\mathrm{mod}}(E)=\Gamma g(E)-\alpha, \tag{5}$$

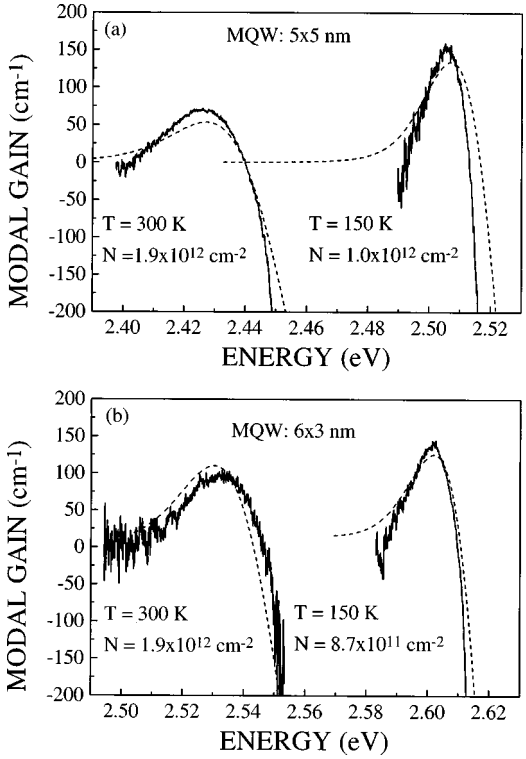

FIG. 6. Measured (solid) and calculated (dashed) optical gain spectra at two different temperatures for the (a) 5×5 nm and the (b) 6×3 nm sample.

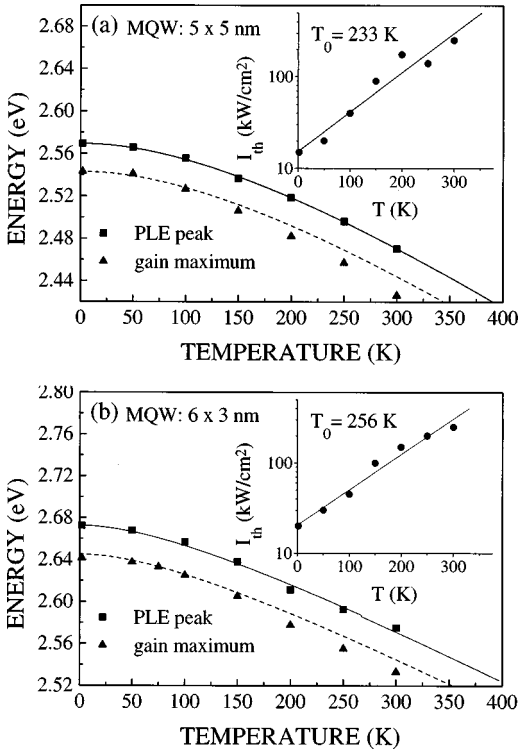

FIG. 7. Temperature dependence of the energy position of the excitonic resonance in the PLE spectra (squares) and of the gain maximum in the VLSM (triangles) for the (a) 5×5 nm and the (b) 6×3 nm sample. Inset: Threshold pump intensities for the onset of optical gain for the corresponding samples.

with Γ the optical confinement factor. The total loss α (caused by scattering of light at crystal defects and by imperfect waveguiding) is assumed to be independent of energy. The confinement factors of the two laser samples were determined from fits to measured far fields, yielding $\Gamma(6\times3\ \text{nm})=0.105$ and $\Gamma(5\times5\ \text{nm})=0.146$. For the 6×3 nm (5×5 nm) sample we get a peak optical gain $g_{\text{peak}}=2900\ \text{cm}^{-1}$ ($1500\ \text{cm}^{-1}$) for an excitation density of 100 kW/cm^2. The larger value for the smaller well width is expected since the quasi-2D density of states increases with decreasing well thickness L_z, being proportional to $1/L_z$.

The gain spectra of both samples for two different elevated temperatures are shown in Fig. 6. The excitation density was chosen to be about two times the threshold density at each temperature. We observe a strong redshift of the gain maxima with increasing temperature, which is mainly determined through the temperature dependence of the band-gap energy and will be discussed below in more detail. The gain spectra of both samples have nearly the same spectral width at 300 K after that of the 6×3 nm sample is clearly broader at low temperature (see Fig. 5), and still somewhat broader at 150 K. This is due to the fact that the spectral shape of the gain at 300 K is mainly determined by carrier-carrier interaction and carrier–LO-phonon scattering masking the original inhomogeneous density of states, which could clearly be seen at 2 K. Another feature of the measured gain spectra is that the experimental low-energy tail is negative. This feature is typical of stripe-length measurements, in which the modal gain extracted is influenced by other loss mechanisms α [see Eq. (5)]. Additionally, we have plotted in Fig. 6 calculated gain spectra using the same material parameters as in the case of the calculated low-density PLE curves in Fig. 3. A detailed discussion of the numerical results will follow in Sec. VI.

The redshifts of the gain maxima near threshold along those of the exciton PLE maxima are plotted as a function of temperature in Figs. 7(a) and 7(b) for both samples. The solid curves are theoretical fits of the positions of the heavy-hole peaks as a function of temperature T, given by the empirical Varshni formula[24]

$$E_{\text{hh}}(T)=E_{\text{hh}}(0)-aT^2/(T+b) \tag{6}$$

with $E_{\text{hh}}(0)=2.569$ eV (2.673 eV), $a=8\times10^{-4}$ eV/K (5.3×10^{-4} eV/K), and $b=433$ K (177 K) for the 5×5 nm (6×3 nm) sample. The dashed curves represent the same fits vertically shifted by the distance PLE peak-gain peak at 2 K to highlight the increasing energetic difference between gain maxima and the low-density hh peaks with increasing temperature for both samples. Accordingly, the threshold pump level for optical net gain increases with increasing temperature as shown in the insets of Figs. 7(a) and 7(b). The threshold dependence on temperature is traditionally discussed in terms of an effective temperature T_0, as a measure of its strength being mainly dependent on the laser material. We have verified that the temperature dependence can be well described by an exponential law[25] in the whole investigated temperature regime (2–300 K),

$$P_{\text{th}}\sim\exp(T/T_0). \tag{7}$$

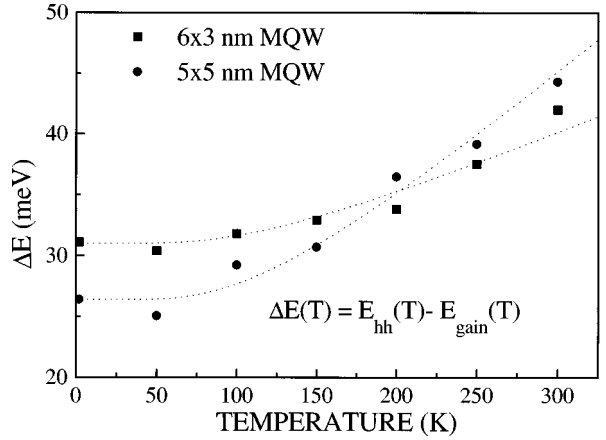

FIG. 8. Temperature dependence of the energy difference between the excitonic resonances in the PLE spectra and the gain maxima for the 5×5 nm and the 6×3 nm samples. The dashed curves are guides for the eye.

The global T_0 value averaged over a large temperature range is 233 K (256 K) for the 5×5 nm (6×3 nm) sample. Only a slight difference ($<10\%$) of the T_0 values is thus obtained for the two samples with different well widths L_z. The values are somewhat smaller than for GaAs/Al_xGa_{1-x}As quantum-well lasers, where T_0 values around 300 K were found under comparable experimental conditions.[26] The (Zn,Cd)Se/Zn(S,Se)/(Zn,Mg)(S,Se) laser structures have therefore a slightly stronger increase in threshold density with temperature than the GaAs/Al_xGa_{1-x}As quantum-well lasers.

Figure 8 shows the temperature dependence of the energy difference ΔE between the gain maxima and the low-density hh peaks for both samples. At low temperatures ($T<50$ K), ΔE is nearly constant and clearly larger for the 6×3 nm sample (31 meV) than for the 5×5 nm sample (24 meV). With rising temperature ΔE increases for both samples, however the slope is larger for the 5×5 nm sample. At 300 K, ΔE reaches a value of about 43 meV for both samples.

V. DISCUSSION

Localization effects due to well-width fluctuations and alloy disorder in ternary QW's make the unambiguous identification of the lasing mechanism in II-VI materials difficult. One has to distinguish between free and localized excitons. If the lasing mechanism involves free excitons, the laser processes can be distinguished spectroscopically by the characteristic energy of the luminescence. There is a wealth of literature comparing the energetic distance ΔE between the heavy-hole–exciton peak and the actual lasing energy. This distance has been used as a measure of the importance or not of excitonic processes in a laser. Now, we will compare our experimental data with the predictions for this distance derived from the models mentioned before, and with the results of the many-body theory including inhomogeneous broadening, which can dramatically increase this distance. A detailed evaluation of this effect is given in the analysis of our theoretical result below. The spectral positions of the stimulated emission at 2 K are 24 meV and 31 meV below the hh exciton peak for the 5×5 nm sample and 6×3 nm sample, respectively. If exciton–LO-phonon scattering would be the mechanism of the stimulated emission, the energetic difference ΔE between the stimulated emission at threshold and the hh exciton peak should equal the LO-phonon energy $E_{\mathrm{LO}}=30$ meV (Ref. 4) and should not depend on the well width. This is in contrast to our findings.

In the case of exciton-exciton scattering one exciton recombines radiatively while the other is scattered into a higher bound state or into the continuum, resulting in the so-called P_2, P_3, and P_∞ bands.[27] For three-dimensional (3D) excitons $E_{1S}-E_{2S}=0.75R_y^{3\mathrm{D}}$, whereas for two-dimensional (2D) excitons $E_{1S}-E_{2S}=0.88R_y^{2\mathrm{D}}$, with E_{1S} (E_{2S}) the $1S$ ($2S$) exciton-state energy and $R_y^{3\mathrm{D}}$ ($R_y^{2\mathrm{D}}$) the 3D (2D) value of the exciton binding energy. For a quasi-2D exciton we would therefore expect the $2S$ exciton state to lie somewhere between $0.75E_b$ and $0.88E_b$ beyond E_{1S}. Taking the lower limit (3D case) ΔE should be found in the range between E_b and $0.75E_b$, which results in values between 24 (27) and 32 meV (36 meV) for the 5×5 nm (6×3 nm) sample. However, exciton-exciton scattering, which seems to be possible from energetic considerations, is excluded since we observe no redshift of the gain spectrum with increasing excitation density (see Fig. 5), which is a characteristic signature for this process due to excitation-induced reabsorption processes.[28]

The exciton-electron process is characterized by a significant temperature-dependent redshift of its emission maximum $\hbar\omega_{\max}$ relative to the heavy-hole excitonic resonance E_{hh},

$$\hbar\omega_{\max}(T)=E_{\mathrm{hh}}(T)-\frac{1}{2}\frac{M_{\mathrm{ex}}}{m_{\mathrm{el}}}k_BT, \tag{8}$$

where M_{ex} and m_{el} are the exciton and the electron masses, respectively. Therefore, exciton-electron scattering should lead to a linear increase of ΔE, which is in contrast to our experimental results at low temperatures (<150 K, see Fig. 8). Even if one fits the temperature shift of ΔE between 150 K and 300 K with a linear regression of Eq. (8), the experimental temperature coefficient of $0.72k_B$ ($1k_B$) for the 6×6 nm (5×5 nm) sample is well below the theoretical one of about 2.6. Therefore, exciton-electron scattering is also excluded at higher temperatures.

Biexcitonic recombination can be excluded since ΔE is much larger than the reported values for biexciton binding energies of 6–15 meV in comparable II-VI heterostructures.[6,29,30] Furthermore, biexcitonic signatures are not visible in edge emission spectra of our samples (see Fig. 2) in contrast to results in extremely pure laserlike structures recently reported by Kreller *et al.*[29] The reason for this different behavior is not finally clear. However, it is probably connected with the larger inhomogeneous broadening of our samples.

The possibility of optical gain at the low-energy tail of a strongly inhomogeneous excitonic density of states has been proposed in ZnCdSe/ZnSe heterostructures by Ding *et al.*[3,4] An unambiguous identification of lasing from excitons in a localizing system such as ZnCdSe/ZnSe multiple quantum wells has been obtained by Cingolani *et al.*[31] by measuring the diamagnetic shift of the stimulated emission being quadratic in magnetic field. From our experimental results we

cannot decide whether the stimulated emission at low temperature is due to localized excitons or due to a gain more driven by an electron-hole plasma. At higher temperatures ($T>60$ K) the excitons are more and more thermally excited into extended states above the mobility edge[27] where they behave at least as free excitons if not as a Coulomb-correlated electron-hole plasma. In this sense, localization should play a reduced role in the recombination process at high temperatures.

Finally, band-to-band transitions of an electron-hole plasma have to be considered. The characteristics of the gain curves in dependence on excitation density favor this type of recombination. The observed shift of the low-energy tail of the gain spectra to lower energies with increasing excitation density (see Fig. 5) can be explained by many-body effects of the electron-hole system, which lead to band-gap shrinkage. Further, the blueshift of the crossover energy from modal gain to absorption can be explained through the high-energy shift of the chemical potential with increasing carrier density. However, the data of the two-beam experiment clearly show that a pronounced excitonlike peak is remaining visible for pump intensities well above the threshold densities. This is not explainable in the framework of a ''free carrier model,'' i.e., without consideration of strong Coulomb correlations between the carriers.

As a conclusion drawn from the up-to-now presented findings in the literature and in this paper, one has to state that neither an excitonic nor a plasma picture of the lasing is capable of explaining consistently the different experimental observations, not even those found in the analysis of one and the same sample. This makes desirable an approach going beyond the limits of the relatively simply structured models used so far.

The microscopic theory summarized in Sec. III provides a more consistent interpretation. The numerical study starts by finding the material parameters applying to the different samples. The homogeneous broadening and band gap as a function of temperature are determined by comparison of the experimentally determined low-excitation PLE with the calculated linear absorption (see Fig. 3). The procedure is justified, since measured absorption spectra (not shown here) have nearly the same spectral shape as the PLE spectra, and no deviations of the maxima in corresponding PLE and absorption spectra are observed.

As previously discussed, the inhomogeneous broadening is caused by well width and alloy concentration fluctuations. For a concrete analysis of inhomogeneous broadening under controlled conditions in our numerical analysis, we take a fixed well width and introduce a Gaussian distribution of the $Zn_xCd_{1-x}Se$ alloy concentration around a central value x_c, $P(x)=P_0\exp[-(x-x_c)^2/x_w^2]$, where x_w characterizes the width of the dispersion. We get the best overall agreement between experimentally and numerically determined line shapes for $x_c=0.84$ (0.8) and $x_w=0.015$ (0.014) for the 6×3 nm (5×5 nm) sample. In other words, inhomogeneous broadening is slightly stronger for the thinner wells. Note that there is a discrepancy between computed and measured high-energy subband peak positions at high temperatures. We attribute this shift to the fact that we assumed, for calculation, the same band-gap shift as a function of temperature for both the well and barrier alloy. The difference, however,

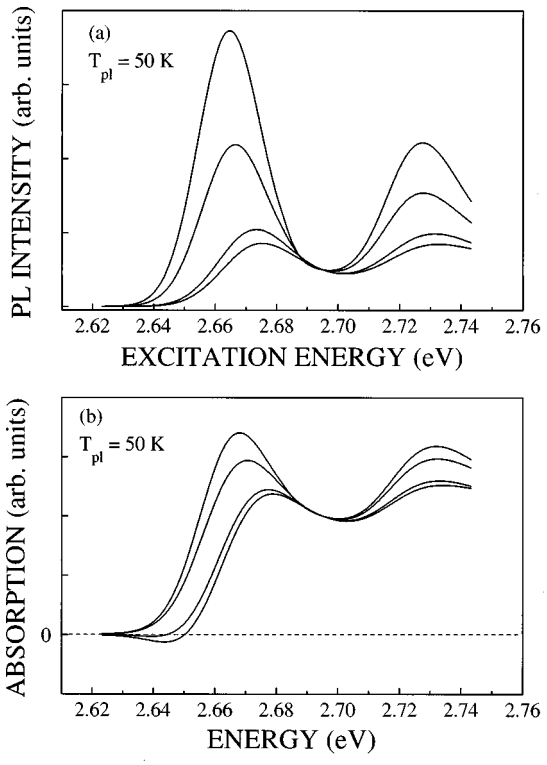

FIG. 9. (a) Two-beam PLE spectra for a 3 nm QW at at plasma temperature $T_{pl}=50$ K. From top to bottom the pump intensities are $P=0.33,0.5,1,2\times P_{th}$. The corresponding absorption spectra, with the same normalization, are shown in (b).

does not affect the following analysis, since we concentrate on the spectral region around the lowest-energy peak. The inhomogeneous broadening determined by x_c,x_w values characterizes the sample as a whole and is kept fixed for all temperatures. The homogeneous broadening, however, exhibits a strong frequency, carrier density, momentum, and temperature dependence. Now, we increase the carrier density until gain develops. The comparison between theory and experiment at elevated temperatures of 150 and 300 K is given in Fig. 6. Good qualitative agreement between theory and experiments is achieved as far as the spectral position and gain linewidth are concerned. However, the negative low-energy tail in the measured gain spectra is not reproduced by the numerical calculation. As mentioned above, loss mechanisms not related to the gain-generating process are responsible for this finding and are not considered in the theoretical model. The good overall agreement between experiment and theory for the low- and high-density spectra demonstrated in this paper shows that the approximations are justified. Since we fix the parameters obtained from the low-density spectra and use them to analyze a broader range of carrier densities, the procedure is meaningful. The computed results thus yield information about the microscopic processes involved. This would not be true if we had adjusted each curve at each density value, since the microscopic information contained in the numerics would have been lost through the fit procedure.

Figure 9 depicts the computed two-beam PLE spectra and corresponding nonlinear absorption spectra for the 3 nm MQW sample at 50 K, simulating the measurement (compare Fig. 4). We do not have access to the actual plasma

temperature, which, however, will definitely be higher than the lattice temperature of 2 K. An intermediate value $T_{\mathrm{pl}} = 50$ K has been selected to illustrate the coexistence of an excitonlike feature and optical gain at low temperatures. The method can be summarized as follows. First, the linear absorption is computed. From that the numbers of carriers generated by the pump can be estimated. Second, the nonlinear absorption and the number of carriers generated by the probe at each excitation frequency are evaluated. The emission intensity due to the total number of carriers is computed at the detection frequency. The luminescence intensity caused by action of the pump only is also calculated and subtracted, giving rise to the differential luminescence presented. The computed spectra consistently reproduce the experimental results depicted in Fig. 4, where the excitonic features are progressively bleached and broadened with increasing pump-generated carrier densities. The coexistence of excitonic features, which we rather interpret in terms of a correlated electron-hole plasma, and gain is evident in the absorption spectra at higher densities.

We would like to point out that spectroscopy is a relevant tool in the study of the microscopic mechanisms that give rise to lasing in II-VI compounds, but has its shortcomings. For example, if the quantum-well width is reduced, the resulting more effective overlap between the carrier wave functions increases the electron-hole binding and consequently the many-body effects in the optical spectra. In other words, the excitonlike features should in principle be more evident in thinner quantum wells. However, thinner samples usually are more strongly inhomogeneously broadened than thicker ones, and the inhomogeneous broadening effects can erase the ''excitonic'' features from an experimental spectrum. The progressive masking of the Coulomb correlation features with increasing inhomogeneous broadening in the absorption and/or gain spectra is depicted in Fig. 10. Moreover, it demonstrates the strong dependence of the peak-gain position on inhomogeneous broadening. As a consequence, it is not adequate to compare samples just on the basis of their nonlinear absorption and luminescence alone if inhomogeneous broadening is a pronounced effect.

In summary, calculations of absorption and gain based on the first-principles theory for light emission and absorption in semiconductors presented here show good agreement with experimental data obtained from II-VI laser structures in the linear and high-density regimes. This provides an interpretation of the mechanism responsible for lasing in II-VI quantum wells in terms of a strongly Coulomb correlated electron-hole plasma. By the detailed theoretical and experimental analysis performed, we have demonstrated the considerable influence of inhomogeneous broadening on the energy difference between the peak gain and the peak of the excitonic absorption. Thus, it is definitely not adequate to deduce an acting lasing mechanism mainly from that particular quantity. We hope that the predicted spectra will stimulate further systematic experimental studies under controlled growth and excitation conditions. The influence of Coulomb correlations in the distribution functions should play a role in the very-low-temperature regime. The full solutions of the self-consistent equations for the self-energy, chemical potentials, and polarization functions are currently being investigated and will be the subject of future publications.

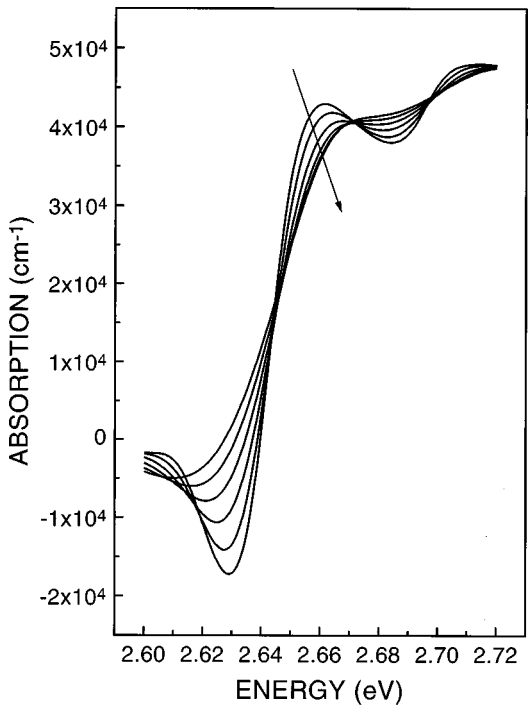

FIG. 10. Absorption spectra for a 3 nm QW at plasma temperature $T_{\mathrm{pl}}=50$ K. A Gaussian distribution is assumed for the concentration fluctuation, $P(x)=P_0\ \exp[(x-x_c)^2/x_w]$. Following the arrow, the inhomogeneous broadening is increased, $x_w = 0.005,0.01,0.015,0.02,0.025,0.03$.

ACKNOWLEDGMENTS

This work was supported by the Deutsche Forschungsgemeinschaft (Grant Nos. He 1975/4, Gu 252/9, and Ho 1388/7).

[1] C. Bénoit à la Guillaume, J. M. Debever, and F. Salvan, Phys. Rev. **177**, 567 (1969).

[2] H. Haug and S. Koch, Phys. Status Solidi B **82**, 531 (1977).

[3] J. Ding, H. Jeon, T. Ishihara, M. Hagerott, A. V. Nurmikko, H. Luo, N. Samarth, and J. Furdyna, Phys. Rev. Lett. **69**, 1707 (1992).

[4] J. Ding, M. Hagerott, T. Ishihara, H. Jeon, and A. V. Nurmikko, Phys. Rev. B **47**, 10 528 (1993).

[5] C. Klingshirn and H. Haug, Phys. Rep. **70**, 315 (1980).

[6] F. Kreller, M. Lowisch J. Puls, and F. Henneberger, Phys. Rev. Lett. **75**, 2420 (1995).

[7] V. Kozlov, P. Kelkar, A. V. Nurmikko, C.-C. Chu, D. C. Grillo, J. Han, C. G. Hua, and R. L. Gunshor, Phys. Rev. B **53**, 10 837 (1996).

[8] R. Cingolani, R. Rinaldi, L. Calcagnile, P. Prete, P. Sciacovelli, L. Tapfer, L. Vanzetti, G. Mula, F. Bassani, L. Sorba, and A.

Franciosi, Phys. Rev. B **49**, 16 769 (1994).
[9] C. Klingshirn, H. Kalt, M. Umlauff, W. Petri, F. A. Majumder, S. V. Bogdanov, W. Langbein, M. Grün, M. Hetterich, K. P. Geyzers, M. Heuken, A. Naumov, H. Stanzl, and W. Gebhardt, J. Cryst. Growth **138**, 786 (1994).
[10] J. Ding, M. Hagerott, P. Kelkar, A.V. Nurmikko, D. C. Grillo, L. He, J. Han, and R. L. Gunshor, Phys. Rev. B **50**, 5787 (1994).
[11] P. Rees, F. P. Logue, J. F. Donegan, J. F. Heffernan, C. Jordan, and J. Hegarty, Appl. Phys. Lett. **67**, 3780 (1995).
[12] A. Girndt, F. Jahnke, A. Knorr, S. W. Koch, and W. W. Chow, Phys. Status Solidi B **202**, 725 (1997).
[13] P. R. Newbury, K. Shahzad, and D. A. Cammack, Appl. Phys. Lett. **58**, 1065 (1991).
[14] Y. Kawakami, I. Hauksson, H. Stewart, J. Simpson, I. Galbraith, K. A. Prior, and B. C. Cavenett, Phys. Rev. B **48**, 11 994 (1993).
[15] A. Dießel, W. Ebeling, J. Gutowski, B. Jobst, K. Schüll, D. Hommel, and K. Henneberger, Phys. Rev. B **52**, 4736 (1995).
[16] K. L. Shaklee, R. E. Nahory, and R. F. Lehny, J. Lumin. **7**, 284 (1973).
[17] M. F. Pereira, Jr. and K. Henneberger, following paper, Phys. Rev. B **58**, 2064 (1998).
[18] K. Henneberger and H. Haug, Phys. Rev. B **38**, 9759 (1988).
[19] M. F. Pereira, Jr. and K. Henneberger, Phys. Rev. B **53**, 16 485 (1996).
[20] M. F. Pereria, Jr., S. W. Koch, and W. W. Chow, J. Opt. Soc. Am. B **10**, 765 (1993).
[21] K. Henneberger and S. W. Koch, Phys. Rev. Lett. **76**, 1820 (1996).
[22] S. Schmitt-Rink, D. S. Chemla, and D. A. B. Miller, Adv. Phys. **38**, 89 (1985).
[23] R. Cingolani, P. Prete, D. Greco, M. Lomascolo, R. Rinaldi, L. Calcagnile, L. Vanzetti, L. Sorba, and A. Franciosi, Phys. Rev. B **51**, 5176 (1995).
[24] Y. P. Varshni, Physica (Utrecht) **34**, 149 (1967).
[25] J. Singh, *Semiconductor Optoelectronics, Physics and Technology* (McGraw-Hill Book Co., Singapore, 1995).
[26] E. Zielinski, H. Schweizer, S. Hausser, R. Stuber, M. H. Pilkuhn, and G. Weimann, IEEE J. Quantum Electron. **QE-23**, 969 (1987).
[27] C. Klingshirn, Adv. Mater. Opt. Electron. **3**, 103 (1994).
[28] M. Umlauff, H. Kalt, C. Klingshirn, M. Scholl, J. Söllner, and M. Heuken, Phys. Rev. B **52**, 5063 (1995).
[29] F. Kreller, J. Puls, and F. Henneberger, Appl. Phys. Lett. **69**, 2406 (1996).
[30] H. Grempel, A. Dießel, W. Ebeling, J. Gutowski, K. Schüll, B. Jobst, D. Hommel, M. F. Pereira, Jr., and K. Henneberger, Phys. Status Solidi B **194**, 199 (1996).
[31] R. Cingolani *et al.*, J. Opt. Soc. Am. B **13**, 1268 (1996).